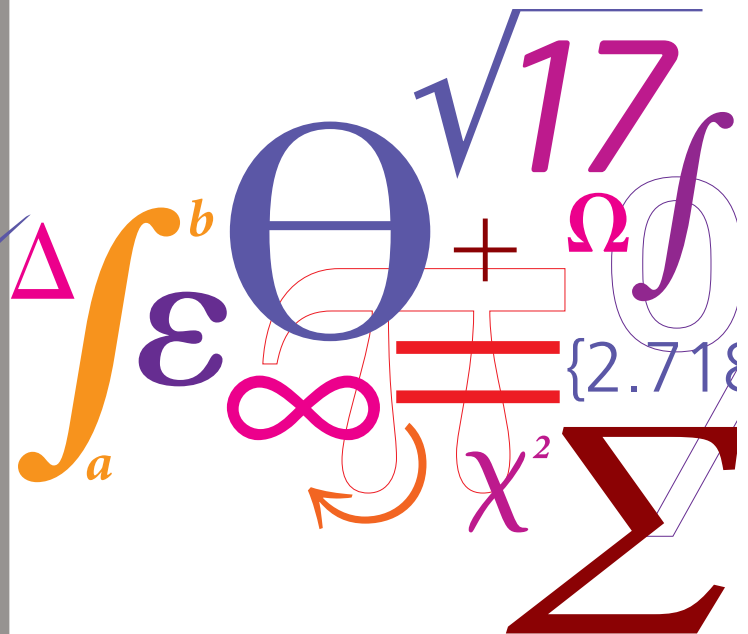


# UniTTe WP3/MC1: Measuring the inflow towards a Nordtank 500kW turbine using three short-range WindScanners and one SpinnerLidar

E-0093

$$P = \frac{1}{2} \rho A v^3 C_p$$



Nikolas Angelou and Mikael Sjöholm  
 DTU Wind Energy  
 September 2015



### **Abstract**

This report provides a description of the experimental setup and the wind scanner remote sensing instruments used in the first measurement campaign of the work package 3 of the UniTTe project. The objective of the campaign was the detailed mapping of the upwind flow in front of a wind turbine. Information regarding the data quality and availability is provided. One of the challenges faced in this experiment was the filtering out of measurements that were biased by the presence of the rotating blades of the wind turbine, in the case where a remote sensing instrument is installed on top of a wind turbine nacelle and pointing upwind. In this report an attempt to realize a blade filtering algorithm is presented along with the corresponding results.

**ISBN:** 978-87-93278-49-3

# Contents

<b>1. Introduction</b>	<b>4</b>
<b>2. Instruments</b>	<b>4</b>
<b>3. Short-range WindScanner</b>	<b>5</b>
3.1. Scanning Patterns . . . . .	5
3.1.1. Scan 1: Horizontal plane . . . . .	5
3.1.2. Scan 2: Vertical plane - perpendicular to the wind turbine rotor . . . . .	6
3.1.3. Scan 3: Vertical plane - parallel to the wind turbine rotor . . . . .	6
3.2. Experimental setup . . . . .	7
3.3. Instrument installation . . . . .	8
3.4. Alignment Evaluation . . . . .	9
3.5. Data post processing . . . . .	10
3.6. Data Overview . . . . .	11
3.6.1. Scanning performance . . . . .	12
<b>4. SpinnerLidar</b>	<b>13</b>
4.1. Steering Calibration . . . . .	14
4.2. Installation . . . . .	15
4.3. Blade filtering . . . . .	18
4.4. Geometrical model . . . . .	19
4.4.1. Model version 1 . . . . .	20
4.4.2. Model version 2 . . . . .	23
4.4.3. Alignment evaluation . . . . .	24
4.4.4. Blade filtering algorithm . . . . .	26
4.5. Overview of the SpinnerLidar measurement campaign . . . . .	29
4.5.1. Measurement range . . . . .	29
4.5.2. Sampling rate . . . . .	30
4.5.3. Scan duration . . . . .	30
4.5.4. Line-of-sight speed, Signal strength and Quality . . . . .	31
4.5.5. Data availability after blade filtering . . . . .	32
<b>Appendix A. Short-range WindScanner database</b>	<b>35</b>
<b>Appendix B. Time lag in the short-range WindScanner data</b>	<b>37</b>
<b>Appendix C. SpinnerLidar database format</b>	<b>40</b>
C.1. The SpinnerLidar Data . . . . .	40
C.1.1. The data columns . . . . .	40

## 1. Introduction

One of the objectives of the research project UniTTe (Unified testing procedures for wind turbines through inflow characterisation using nacelle lidars) is to investigate the interaction between a wind field and an operating wind turbine. In this context and as a part of the Work Package 3 (WP3) a measurement campaign (MC1) was performed using multiple scanning wind light detection and ranging (lidar) instruments. In specific, 3 short-range WindScanners were installed on the wind turbine testing area located in the DTU Risø campus, along with a SpinnerLidar which was mounted on the nacelle at a NordTank wind turbine.

## 2. Instruments

The short-range WindScanner and the SpinnerLidar are remote sensing instruments developed in the Wind Energy Department of the Danish Technical University (DTU) in the framework of the *WindScanner.dk*[2] and the *Integration of Wind Lidar In Wind Turbines for Improved Productivity and Control*[3], research projects respectively. Both instruments consist of two main components, a modified version of a commercial ZephIR wind lidar (ZephIR Ltd., UK) and a scanner head (IPU, DK). The modifications applied to the ZephIR had as an objective to provide a high streaming rate of laser Doppler spectra, as well as, to allow the synchronization of the data acquisition with the scanner head.

The lidar was designed following the principles of a continuous wave (cw), coherent Doppler lidar, which can measure the speed and direction of the wind[1]. This is achieved through the emission of infrared (IR) laser radiation, with a  $1.5 \mu\text{m}$  wavelength, in the atmosphere and subsequently by detecting the radiation backscattered from aerosols. The backscattered signals are sampled at a frequency of 100 MHz and a 512-point Fast Fourier Transform (FFT) is being applied in real time to produce approximately 200000 laser Doppler spectra per second.

The laser Doppler spectra contain information of the Doppler frequency shift of the transmitted radiation induced by aerosols which are blown by the wind. In specific they describe the mean wind speed projected to the line-of-sight of the instrument over the probe length. The probe length is defined by the distribution of the laser light intensity around the focus point, which follows a Lorentzian weighting function[4].

The scanner head consists of two prisms, of a  $30^\circ$  and  $15^\circ$  deflection angle in the case of the WindScanner and SpinnerLidar, respectively. In the case of the WindScanner the prisms are driven separately to steer the lidar's line-of-sight within a cone with a full open opening angle of  $120^\circ$ . While in the SpinnerLidar the scanner head the two prisms rotate in a constant speed, with a fixed speed ratio between them (13/7).

The determination of the measurement distance from the instrument is achieved by altering the position of the fiber end of the output IR laser radiation from an optical lens. The design of the focus mechanism allows a minimum focusing distance of approximately 8 m.

### 3. Short-range WindScanner

The scanner head of the short-range WindScanner consists of two motors, which are used to drive separately each of the two optical prisms. Assuming that the instrument is installed in a vertical position, pointing upwards, it is possible to steer the line-of-sight of the lidar anywhere inside a truncated cone. The base of the cone has a spherical shape, the dimensions of which are defined by the maximum deflection angle of the line-of-sight ( $2 \times 30^\circ = 60^\circ$ ) and the minimum focus distance (8 m) (see Figure 1). The upper limit of the cone is limited in practice due to the increase of the probe volume with distance ( $\propto r^2$ ). The current characteristics of the optical components used in the WindScanner make reasonable its use when measuring up to a distance of approximately 150 m, above that the probe volume is getting larger ( $\geq 30$  m) than of a pulsed lidar scanning system, i.e. long-range WindScanner and thus the spatial filtering is considered to be extensive.

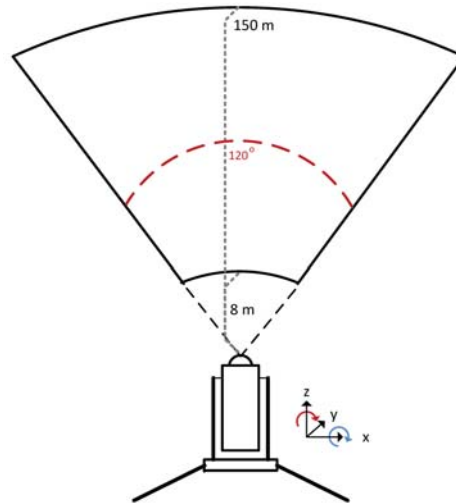


Figure 1: A drawing of the area which describes the scanning limits of a short-range WindScanner.

#### 3.1. Scanning Patterns

For the needs of the experiment, 3 different scanning patterns, each one of a 30 minutes duration, were utilized. Due to different requirements in the motion (velocity and acceleration) of the motors for the realization of each pattern the time of completion of one full scan pattern differs. The scanning patterns were performed using a fixed coordinate system, thus they were not following the wind turbine yaw.

##### 3.1.1. Scan 1: Horizontal plane

The first scanning pattern consisted of 11 lines confined in a horizontal plane, extending from the rotor plane up to 62 m away (see Figure 2). The horizontal distance between each line is 4 m and the time of completion of one scan is approximately 15 seconds. The goal of this scan is to monitor the induction of the wind flow in a horizontal plane.

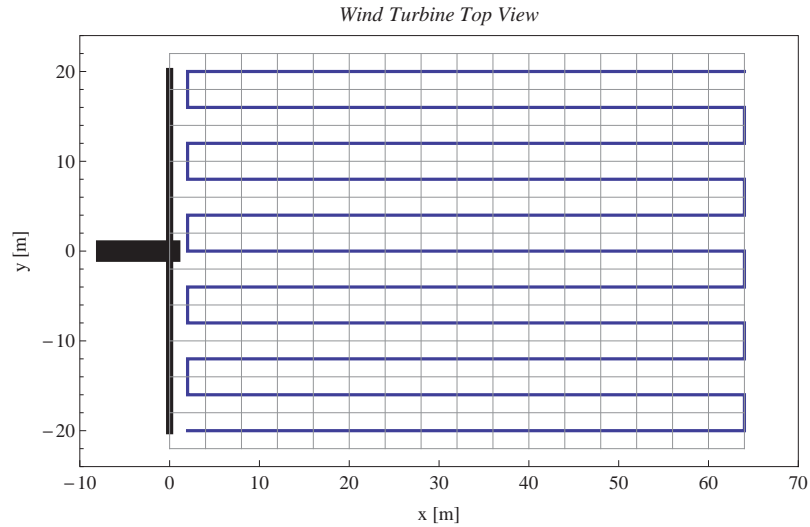


Figure 2: Scan 1: Horizontal plane.

### 3.1.2. Scan 2: Vertical plane - perpendicular to the wind turbine rotor

The second scan is a vertical plane which consists of 11 lines, extending from the rotor plane up to 62 m away (see Figure 3). The vertical distance between each line is 4 m and the time of completion of one scan is approximately 30 seconds. The goal of this scan is to monitor the induction of the wind flow in a vertical plane.

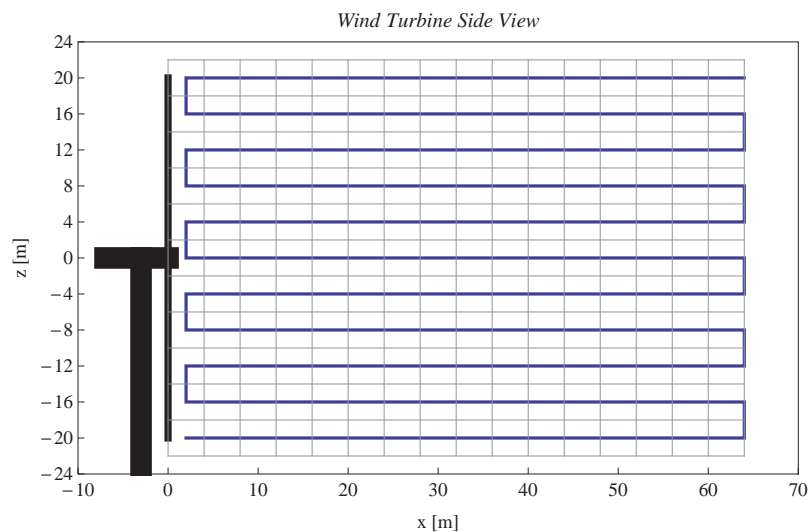


Figure 3: Scan 2: Vertical plane.

### 3.1.3. Scan 3: Vertical plane - parallel to the wind turbine rotor

The third scan is a vertical plane parallel to the rotor plane. The scan follows a rose pattern which is confined within the  $\frac{2}{3}$  of the radius of the wind turbine rotor (see Figure 4). The time of completion of one scan is approximately 6 seconds. The goal of this scan is to attempt to investigate the coherence of the wind flow in different parts of the wind turbine rotor when the flow is already affected by the induction zone.

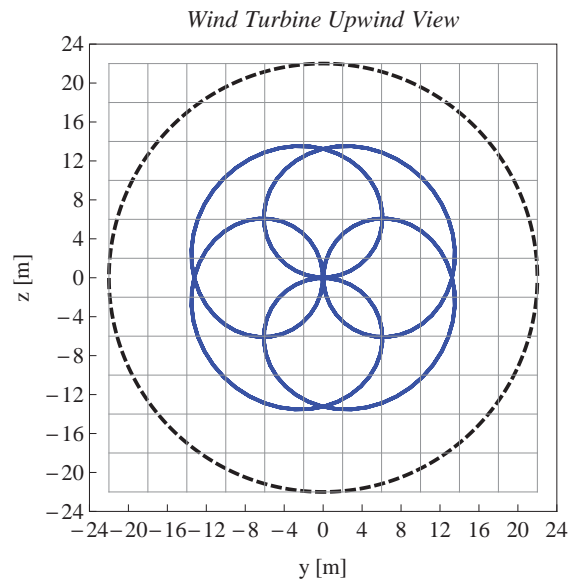


Figure 4: Scan 3: Vertical plane parallel to the wind turbine rotor.

### 3.2. Experimental setup

Based on the specifications of the 3 different scanning patterns, it was determined the location of the positions, where the short-range WindScanners would be deployed. The criteria used were: a. installing the instruments close to the scanning area to insure as short as possible lidar probe lengths and b. the velocity and acceleration of the motors' motion should be lower than the limits specified in the operational parameters. The location were measured using a total station theodolite (TST). As a reference point it was used a point on the staircases (102 cm above ground) which leads to the door of the wind turbine (see Figure 5).



Figure 5: Photo of the NordTank wind turbine used during the measurement campaign. The use point used as a reference for the TST is presented in a zoomed frame. Behind the wind turbine one the short-range WindScanners (R2D1) can be seen.

### 3.3. Instrument installation

The short-range WindScanners were deployed at the DTU Risø campus the last week of July 2014 and aligned accordingly so as their pointing directions would intersect at a position 36 m above the wind turbine ground level, over the location where the short met mast was found. Following the installation of the WindScanners their location and tilt angle were measured using a TST and a digital inclinometer, respectively. The results relative to the location of the wind turbine  $\{0, 0, 0\}$  and assuming a right-hand Cartesian coordinate system, whose positive x-axis is pointing towards the two met masts, are presented in the Figure 6. The origin of the coordinate system was measured by a TST to be +0.15 m, along the x-axis, away from the center of the rotor plane.

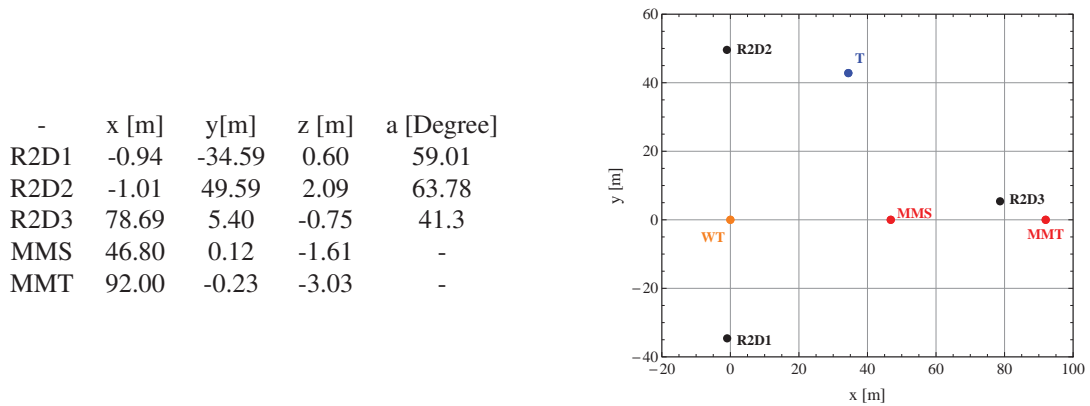


Figure 6: Coordinates (left) and the corresponding drawing (right) of the location of the 3 short-range WindScanner (R2D1, R2D2 and R2D3), the two met mast (MMS and MMT) and of the TST (T).

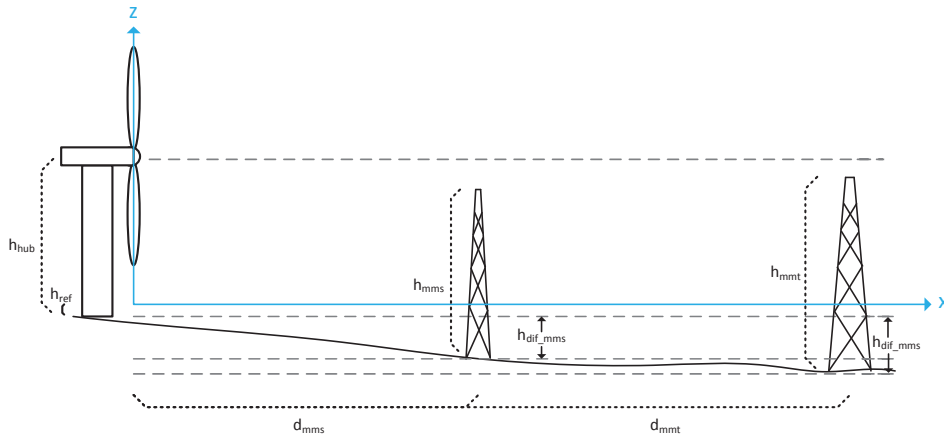


Figure 7: Side view of the wind turbine and the two met masts, where the height differences between them are presented.

$h_{ref}$ [m]	$h_{dif_{mms}}$ [m]	$h_{dif_{mmt}}$ [m]	$h_{mms}$ [m]	$h_{mmt}$ [m]
0.46	1.98	-3.27	-	-

Table 1: mpla

### 3.4. Alignment Evaluation

To evaluate the alignment of the short-range WindScanners, a rotating ball (30 cm diameter) was temporarily installed on top of the short met mast and consequently it was scanned. The rotating ball location was also measured using a TST and it was found that it was located 30.6 m above the ground level of the wind turbine (see Figure 8).

The rotating ball was found to be at a height of 30.36 m, 30.37 m, 30.46 m from R2D1, R2D2 and R2D3 respectively (see Figure 9). These heights indicate an offset of the tilt angle of the instruments of  $0.18^\circ$ ,  $0.16^\circ$  and  $0.12^\circ$  respectively. The distance between the WindScanner units and the rotating ball was 65.9, 74.3 and 44.5 m.



Figure 8: Photo of the one of the short-range WindScanners used (R2D2) and of the short met mast. The rotating ball installed on the short met mast appears to the right.

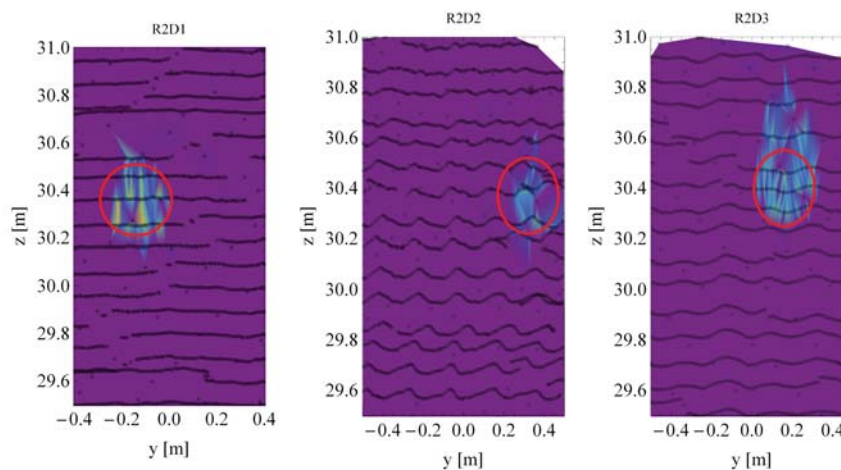


Figure 9: Plots of the signal intensity in the laser Doppler spectra acquired from each of the 3 short-range WindScanners.

### 3.5. Data post processing

The data acquired from the short-range WindScanners were grouped in grid cells (see Figures 10) and a spatial averaging was performed per grid cell. The averaging was performed both per turn but also per iteration. Consequently the radial wind speeds acquired of each one of the short-range WindScanners were used to estimate the 3 components ( $u$ ,  $v$ ,  $w$ ) of the wind vector.

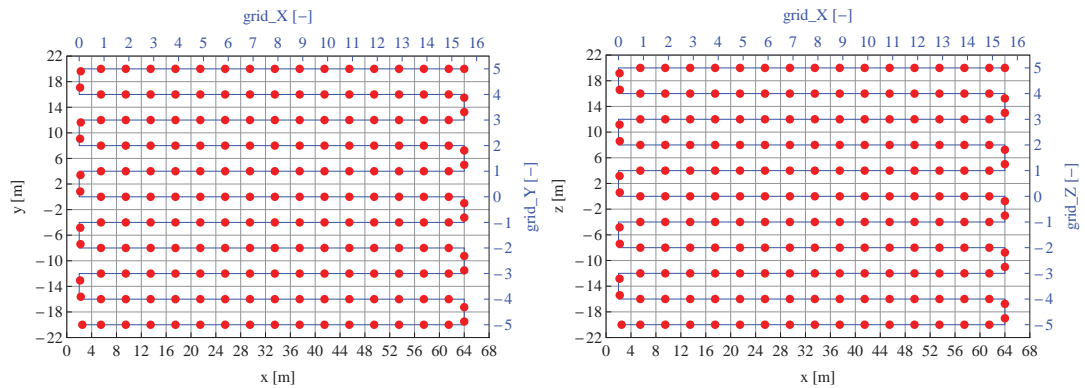


Figure 10: The horizontal plane scan #1 (left), the vertical plane scan #2 (right), the vertical plane parallel #3 (bottom) to the wind turbine rotor and their corresponding grids.

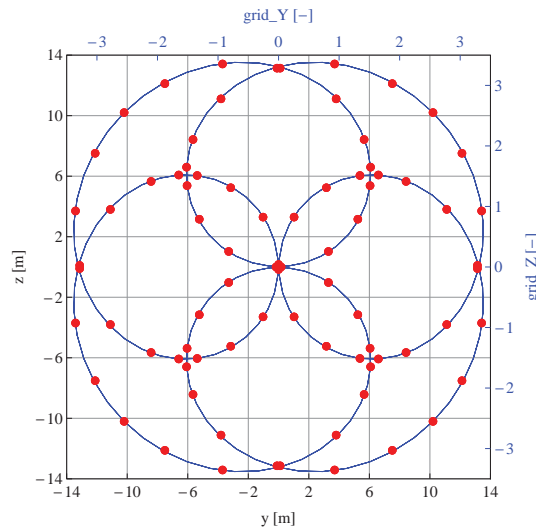


Figure 11: Scan 3: Vertical plane parallel to the wind turbine rotor and corresponding grid.

### 3.6. Data Overview

The total amount of the data acquired during the experiment are presented in the Table 2, where the number of 30-min periods per date and per scan are presented.

Date	Scan Index			
	1	2	3	4
20140806	1	2	2	0
20140820	1	4	4	0
20140821	1	6	5	0
20140825	1	2	2	0
20140827	1	0	0	0
20140828	0	6	6	0
20140925	1	7	7	0
20140927	3	2	1	0
20141002	1	1	1	0
20141029	7	6	0	0
20141030	6	6	0	0
20141031	0	0	0	7
20141103	0	0	0	9
Total	23	42	28	16

Table 2: Total amount of data in number of 30-min periods.

The data for each one of the above dates are stored in a separate table in the database (see Appendix A. The scan indexes 1, 2 and 3 correspond to the 3 different scanning patterns used. The scanning index 4 refers to measurements taken on a staring mode, while the line-of-sights of the 3 short-range WindScanners intersected over the sonic anemometer of the short met mast. The data acquired on the 29th and 30th of April were taken while the test wind turbine was not operating. The objective was to attempt to investigate how the terrain is affecting the wind flow. During the measurement campaign it was observed that the computer used to log the data was drifting in time, creating a time lag between the WindScanner, the met mast and the wind turbine data. The time series of the estimated time lags are presented in the Figure 12 and in Appendix B.

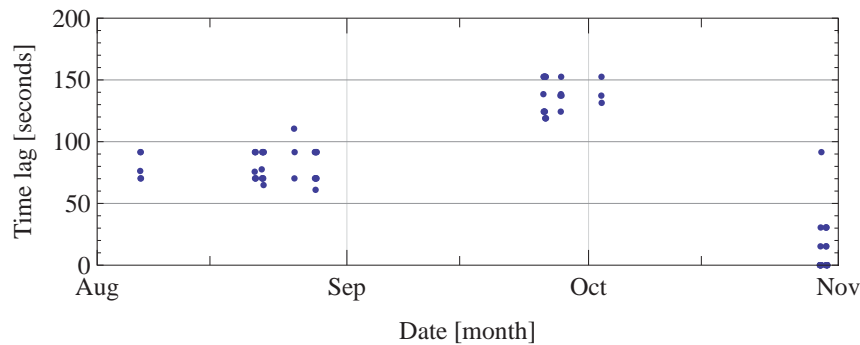


Figure 12: Time series of the estimated time lag between the computer that acquired the short-range WindScanner and the met mast data acquisition system.

### 3.6.1. Scanning performance

During the experiment, two of the instruments (R2D2 and R2D3) appeared to have a degrading performance in the accurate completion of the scanning pattern. This was observed due to sporadic malfunction of the mechanism used to define the distance away from the instrument where the measurements were taken. The result of this error is that during the iteration of one scanning pattern one of the instrument could not follow the commanded scanning pattern. Such an event would lead to mismatch in the location of the synchronous measurements from the 3 instruments and thus the amount of the data available per scan would be less than the expected one. The periods when such events were observed are presented in the following table.

R2D2	
20140806	11:01 - 12:31
20140828	12:42 - 12:57
20140927	13:49 - 14:19
	15:31 - 15:58
	17:13 - 17:36
20141002	14:08 - 14:31
R2D3	
20140820	12:23 - 13:25
20140821	10:19 - 11:21
20140825	10:41 - 11:38
20140925	09:56 - 17:59
20140927	12:11 - 18:59
20141029	17:30 - 23:59
20141030	10:54 - 12:25

Table 3: Periods where either R2D2 or R2D3 were malfunctioning.

## 4. SpinnerLidar

The SpinnerLidar is a remote sensing instrument developed to scan the wind inflow towards a wind turbine rotor when installed either in the spinner of a wind turbine hub or on top of the nacelle (see Figure 13).



Figure 13: The SpinnerLidar installed on top of the NordTank turbine at DTU Risø campus.

The scanner-head of the SpinnerLidar consists of two optical prisms with a deflection angle of  $15^\circ$ . The two prisms rotate in a constant speed, with a fixed ratio between them (13/7). When the measurement distance away from the instrument is fixed, then the rotating prisms steer the laser beam in a scanning pattern similar to a rose curve with a  $k=13/7$  (see Figure 14).

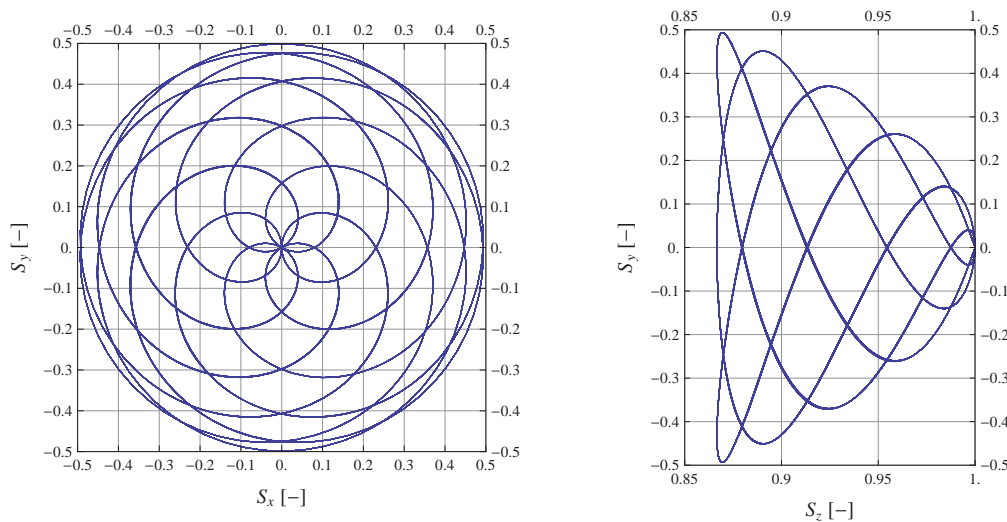


Figure 14: A downwind view of the scanning pattern performed by the SpinnerLidar.

The SpinnerLidar has an internal coordinate system that is such that the z-axis is along the pointing direction of the instrument, the x-axis is looking upwards and the y-axis is the lateral direction. The projections of the unit vector  $\mathbf{n}$  along the line-of-sight

measurement direction on the SpinnerLidar to the 3 axis of a left-handed coordinate system are denoted  $S_x$ ,  $S_y$  and  $S_z$ , respectively. In order to transform the SpinnerLidar coordinate system to a right-handed coordinate system whose x axis will be horizontal, like the one presented in Figure 14, the following rotation has to be applied:

$$\mathbf{n}' = R_z \left( -\frac{\pi}{2} \right) \begin{bmatrix} 1 \\ -1 \\ 1 \end{bmatrix} \mathbf{n}, \quad \text{where } \mathbf{n} = \begin{bmatrix} S_x \\ S_y \\ S_z \end{bmatrix} \quad (1)$$

In all the following figures the  $S_x$ ,  $S_y$  and  $S_z$  notation correspond to the transformed  $\mathbf{n}'$  unit vector.

#### 4.1. Steering Calibration

Prior to the installation of the SpinnerLidar on the NordTank wind turbine it was necessary to estimate the expected accuracy of the location of the measurements acquired while scanning the inflow wind.

**Step 1** In order to determine the alignment of the SpinnerLidar with the upwind direction of the wind turbine a red pointing laser was installed at a distance of 15 cm from the center of the top window of the SpinnerLidar (see Figure 15).

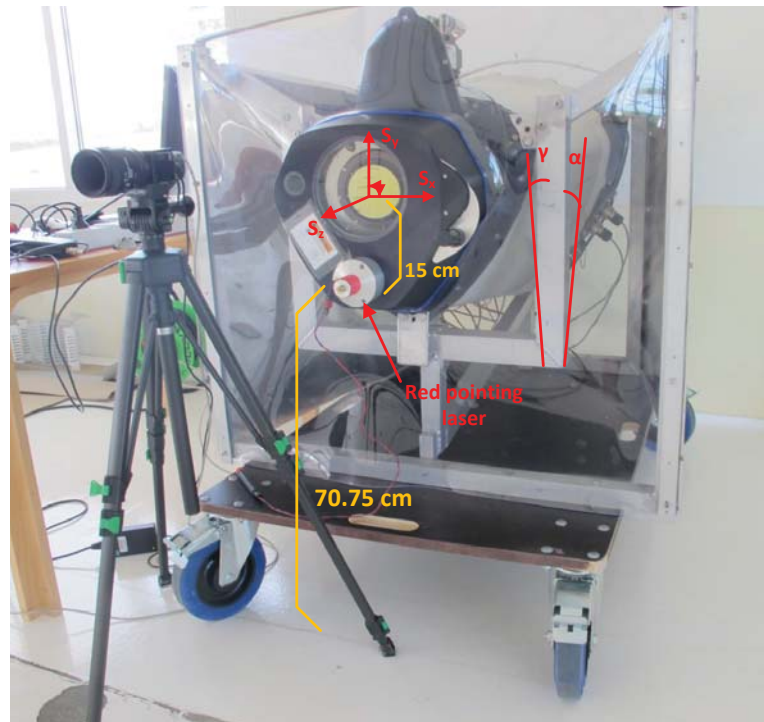


Figure 15: Photo of the SpinnerLidar mounted on the frame used to install the instrument on the wind turbine nacelle.

**Step 2** The angles of the frame used to mount the instrument were measured, relative to a 3-axis right handed coordinate system, whose z-axis is found along the pointing direction of the instrument and the y-axis is pointing upwards (see Figure 15).

According to the measurements of a digital inclinometer these angles are:

Angle	[ $^{\circ}$ ]
$\alpha$	1.3
$\gamma$	0.3

Table 4: Offset angles of the frame to which the SpinnerLidar was mounted.

**Step 3** Using an IR camera (visible on the left of Figure 15) the trace of the laser beam of the SpinnerLidar was recorded on a wall 13.2 m away, while the instrument was scanning. The IR camera was acquiring frames at 50 Hz for a duration of 2 minutes.

**Step 4** The frames were superimposed one on top of the other in an attempt to reconstruct the scanning pattern of the SpinnerLidar (see Figure 16). In the Figure 16 are included both the location of the red pointing laser (red dot), as well as the theoretical position of the center of the scanning pattern (gray dot). The height from the ground of the position of the red pointing laser and the one of its trace on a wall 13.2 m away, were measured to be 70.75 cm and 69 cm, respectively, indicating an tilt angle of  $0.07^{\circ}$  in either the room's floor level or in the line-of-sight of the red pointing laser.

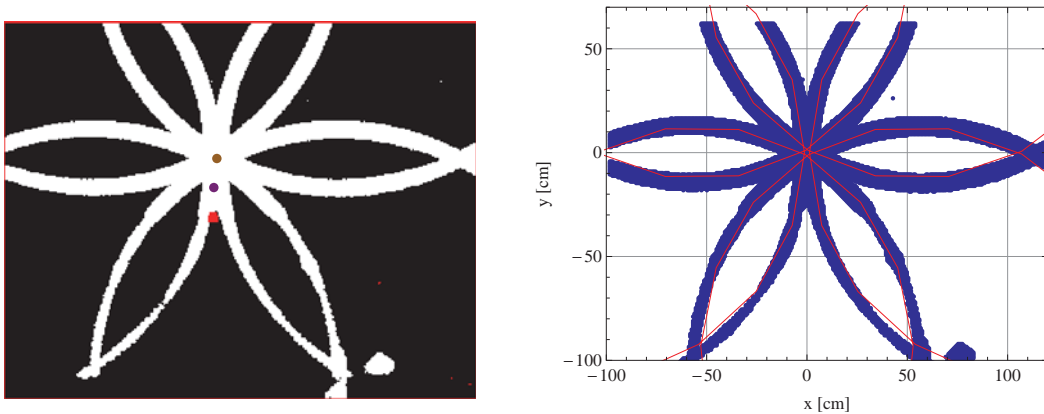


Figure 16: (Left) The scanning pattern of the spinnerLidar based on the trace of the laser beam which was monitored through the use of an IR camera. (Right) The measured scanning pattern (blue) in comparison with the theoretical expected scanning pattern (red).

The center of the SpinnerLidar scanning pattern appears to be 28.6 cm above the red pointing laser beam, instead of 15 cm (purple dot in Figure 16). This indicates that there is an offset of  $0.59^{\circ}$  from the pointing direction of the instrument. In the lateral direction the corresponding distance was measured to be 1.42 cm, which could be due to a slight offset of the pointing direction of the red pointing laser relative to the pointing direction of the SpinnerLidar, due to a rotation around the z axis of the whole instrument, or even both.

## 4.2. Installation

Furthermore it was important to evaluate the accuracy of the alignment of the SpinnerLidar with the yaw direction of the wind turbine. This was tested after the instrument was installed on the wind turbine by measuring the location of both the red pointing laser

on the SpinnerLidar and at a distance of 10 m away from the wind turbine using a differential GPS. The measurements relative to an arbitrary reference point are presented in the following table.

GPS	SpinnerLidar	laser beam trace (10 m away)	Difference
North [m]	140605.174	140597.617	-7.56
East [m]	-101732.796	-101740.306	-7.51
M.S.L. [m]	46.508 (46.928-0.42)	46.758	0.25

Table 5: GPS measurements of the position of the pointing laser beam trace in two locations, right after the SpinnerLidar and at 10 m away respectively.

The measurements were taken when the wind turbine was yawed at  $226.52^\circ$ . The measurement of the height above the Mean Seal Level (MSL) of the SpinnerLidar was taken by placing the GPS antenna on top of the frame used to cover it. It is worth mentioned that the distance between the red pointing laser beam and the top of the antenna was 0.47 m. Additionally the GPS measurements of the MSL are calculated using the bottom of the antenna whose height is approximately 0.05 m. Therefore the measurement of the red pointing laser beam at the SpinnerLidar should be corrected by subtracting  $0.47 - 0.05 = 0.42$  m.

In the Figure 17 the locations noted in the Table 5 are presented. The North is aligned with the positive y-axis and the SpinnerLidar position is set to  $\{0, 0\}$ .

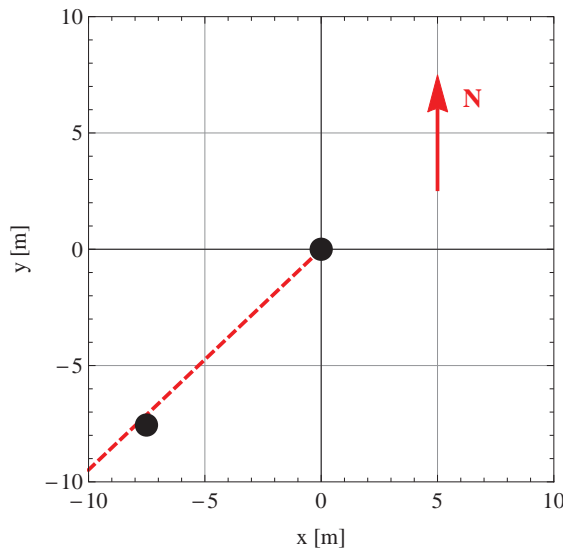


Figure 17: Drawing of the yaw direction of the wind turbine (red dashed line) during the evaluation of the relative alignment of the SpinnerLidar. The two black dots indicate the position where the red pointing laser beam trace was found.

In order to estimate the offset angle of the red pointing laser to the yaw  $\beta$  direction of the wind turbine the following steps were performed:

1. Rotate the coordinate system round the z axis, to align the yaw direction to the x-axis using the following rotation matrix  $R_z(226.52^\circ - 90^\circ)$ . The new coordinates of the position of the trace of the red pointing laser are then  $\{10.64, 0.31\}$ .

2. The rotation  $\beta$  around the y axis it will therefore be equal to the inverse tangent of the rotated coordinates of the position of the red pointing laser.

$$\arctan\beta = \frac{0.31}{10.64} \implies \beta = 1.69^\circ \quad (2)$$

The corresponding vertical displacement angle is equal to:

$$\arctan\alpha = \frac{0.25}{\sqrt{10.64^2 + 0.31^2}} \implies \alpha = 0.25^\circ \quad (3)$$

Therefore, when taking into account also the results of the steering calibration the estimated offset angles, relative to the 3 axis of the coordinate system used, of the pointing direction of the SpinnerLidar's laser beam from to the wind turbine rotor are:

Angle	[°]
$\alpha$	1.3
$\beta$	1.69
$\gamma$	-0.84 (0.59+0.25)

Table 6: Estimated rotation angles of the pointing direction of the SpinnerLidar's laser beam relative to the 3 axis of the coordinate system.

Furthermore, using the measurements from a theodolite it is estimated, that the position of the SpinnerLidar to be  $h = 1.75$  m higher and  $d = 0.98$  m away from the center of the rotor measured by a TST.

### 4.3. Blade filtering

The SpinnerLidar has been developed to be installed in the spinner of a wind turbine, providing this way an unobstructed view of the incoming flow. However, during this campaign the SpinnerLidar was placed on top of the nacelle, behind the rotor and thus the laser transmission was occasionally blocked by the blades of the turbine. Therefore the provided wind measurements were contaminated by spurious values corresponding to signals that originated from the rotating blades rather than aerosols, which should be filtered out.

The signal strength could theoretically provide a discrimination possibility since usually the signal strength from a moving hard target (e.g. blade) is much higher than that from the aerosols. In Figure 18 an example of the relation between the line-of-sight speed and signal strength is given for the data of a 10-min period. The line-of-sight radial speeds ( $V_{r}$ ) which correspond to wind speed measurements appear to vary between  $3 \text{ ms}^{-1}$  and  $14 \text{ ms}^{-1}$ , while the ones that are a result of blade returns are lower than  $3 \text{ ms}^{-1}$ . However as observed, it is not possible to find a demarcation between them, while using only the power of the signal, since there are signal power values that originate both from aerosols and blades. This occurs, due to the fact that first the laser beam close to the instrument is not focused, thus the intensity of the back-scattered signal is not necessary high and furthermore the relative angle between the laser's line-of-sight and blade can be such that limits the amount of back-scattered light.

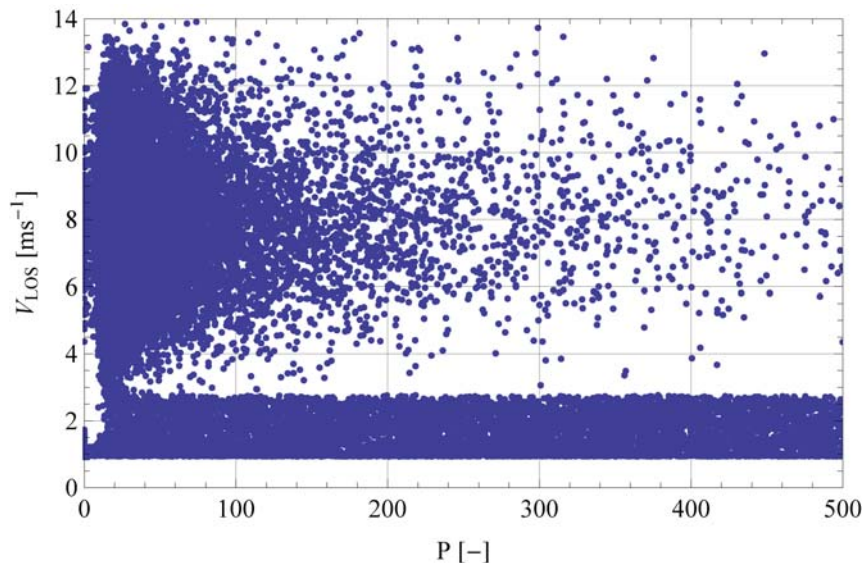


Figure 18: The line-of-sight speed vs the signal strength ( $P$ ) as measured on 2014-08-10 between 23:30 and 23:40.

A method to circumvent this issue is to estimate all the expected radial velocities measured by the SpinnerLidar, when taking into account the position and direction of the SpinnerLidar relative to the axis of rotation of the wind turbine blades, the rotation speed of the rotor and the scanning direction of the line-of-sight of the SpinnerLidar. This calculation can provide a tool to be used for the filtering out the blade return signals.

## 4.4. Geometrical model

In order to implement such a filtering method it will be used a coordinate system whose origin is located at the point of the transmission of the SpinnerLidar's laser beam, and the following parameters (see also Figure 19):

- $\omega$ : angular velocity of the wind turbine's rotor.
- $h$ : height (along the y axis) of the origin of the laser transmission of the SpinnerLidar from the center of the rotor.
- $d$ : distance (along the z axis) of the origin of the laser transmission of the SpinnerLidar from the center of the rotor.
- $l$ : distance (along the x axis) of the origin of the laser transmission of the SpinnerLidar from the center of the rotor.
- $r$ : radial vector from the center of the rotor where the laser beam intersects the wind turbine's rotor.
- $f$ : vector of the line-of-sight of the SpinnerLidar where the laser beam intersects the wind turbine's rotor.

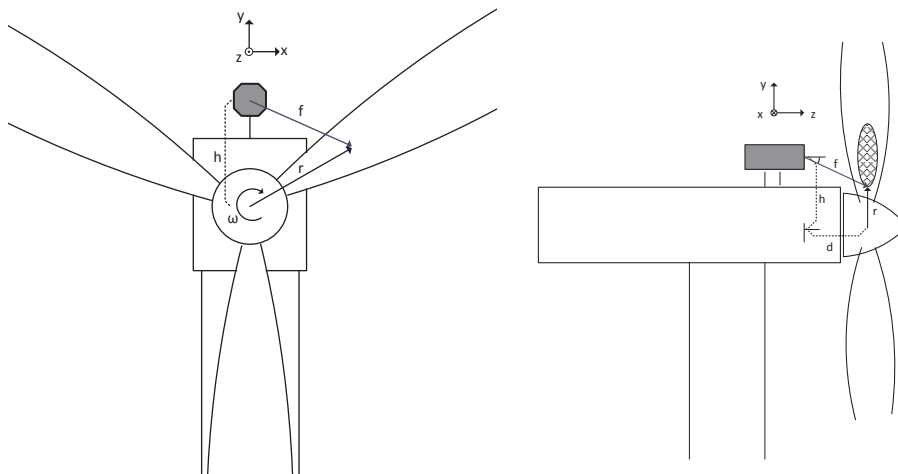


Figure 19: Schematic of the parameters used for the creation of a filtering algorithm depicted on a front (left) and side (right) view of the wind turbine.

#### 4.4.1. Model version 1

As already mentioned, the unit vector  $\mathbf{n}$  which corresponds to the line-of-sight direction of the laser transmission of the SpinnerLidar is defined by  $\{S_x, S_y, S_z\}$ . The  $S_x$ ,  $S_y$  and  $S_z$  can be expressed in spherical coordinates as  $\{\cos\phi\sin\theta, \sin\phi\sin\theta, \cos\theta\}$ , where  $\theta$  is the polar angle and  $\phi$  the azimuth angle (see Figure 20).

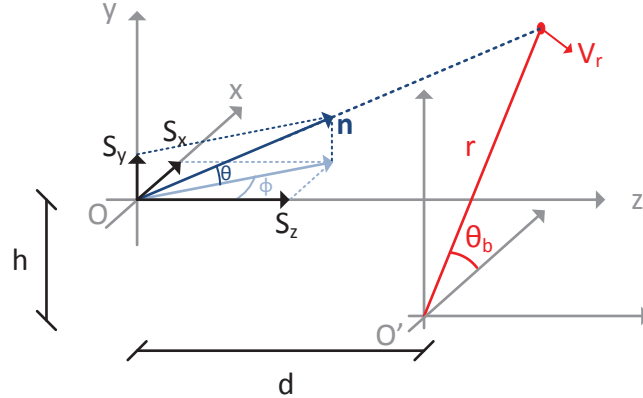


Figure 20: Drawing of the geometrical model which depicts the intersection of the line-of-sight of the laser beam with a rotating blade.

Let denote  $\mathbf{f}$  as the vector which describes the point where the line-of-sight of the SpinnerLidar intersects with the blade of the wind turbine and  $x_f$ ,  $y_f$  and  $z_f$  the corresponding coordinates. Then  $\mathbf{f}$  is defined by the distance  $d$  between the SpinnerLidar and the center of rotation of the wind turbine blade, as well as, the azimuth  $\phi$  and elevation angles  $\theta$  by the following equation:

$$\mathbf{f} = \{d \cdot \tan\phi \cdot \cos\theta, d \cdot \tan\phi \cdot \sin\theta, d\} \quad (4)$$

Assuming that the SpinnerLidar is displaced from the center of the wind turbine rotor only along the vertical  $y$  axis by  $h$ , then the radial vector  $\mathbf{r}$  is defined as:

$$\mathbf{r} = \{d \cdot \tan\phi \cdot \cos\theta, d \cdot \tan\phi \cdot \sin\theta + h, d\} \quad (5)$$

Furthermore, assuming that the blades are rotating in the  $xy$  plane (i.e. ignoring the expected  $2^\circ$  tilt angle of the rotor relative to the tower of the wind turbine) then the radial speed of the blade is equal to:

$$\mathbf{V}_r = \{\omega \cdot r \cdot \sin(-\theta_b), \omega \cdot r \cdot \cos(-\theta_b), 0\} \quad (6)$$

where  $r$  is the radial distance from the center of rotation  $O'$ ,  $\omega$  is the angular speed of the wind turbine blades, and  $\theta_b$  is the angle between the blades and the  $x$ -axis (see Figure 20). Assuming a right-handed coordinate system the blades are rotating clockwise and thus the  $\theta_b$  is getting a negative sign. Moreover the  $\sin\theta_b$  and  $\cos\theta_b$  are equal to:

$$\sin\theta_b = \frac{d \cdot \tan\phi \cdot \sin\theta + h}{r} \quad \text{and} \quad \cos\theta_b = \frac{d \cdot \tan\phi \cdot \cos\theta}{r} \quad (7)$$

The line-of-sight speed measurement of the SpinnerLidar ( $V_{LOS}$ ) is the result of the scalar projection of the radial speed of the blade to the vector of the line-of-sight  $p$ :

$$\begin{aligned}
 V_{LOS} &= \frac{\mathbf{f} \cdot \mathbf{V}_r}{|\mathbf{f}|} \\
 \text{Eq.(0)} \quad &= \frac{-d \cdot \tan\phi \cdot \cos\theta \cdot \omega (d \cdot \tan\phi \cdot \theta + h) + d \cdot \tan\phi \cdot \sin\theta \cdot \omega \cdot d \cdot \tan\phi \cdot \cos\theta}{d \cdot \sqrt{\tan^2\phi + 1}} \\
 &= -\frac{\tan\phi}{\sqrt{\tan^2\phi + 1}} \cdot \cos\theta \cdot \omega \cdot h \\
 &= -\sin\phi \cdot \cos\theta \cdot \omega \cdot h \\
 &= -S_x \cdot \omega \cdot h
 \end{aligned} \tag{8}$$

According to the above equation, it appears that for a specific angular velocity  $\omega$  and vertical displacement  $h$  of the SpinnerLidar relative to the wind turbine rotor, the expected radial speed measurements that will originate from blades should have a linear dependency to the  $S_x$  and be independent from the distance from the wind turbine rotor. In the Figure 21 the radial speed measurements of the SpinnerLidar vs. the  $S_x$  parameter are presented for the same data period as in the Figure 18. It can be observed that below  $3 \text{ ms}^{-1}$  the measured radial speeds recorded are indeed increasing linearly as the  $S_x$  increasing. It has to be noted here that first the SpinnerLidar cannot differentiate the sign of the speed and second that there is a minimum detectable wind speed limit. The latter occurs due to a suppression of any signals appearing with the first 5 frequency bins (0 - 1 MHz) of the calculated laser Doppler spectrum, which results in a minimum detectable speed of  $0.92 \text{ ms}^{-1}$ . This is consistent with the distribution of the radial wind speeds that are reported in Figure 21 (see red dashed line).

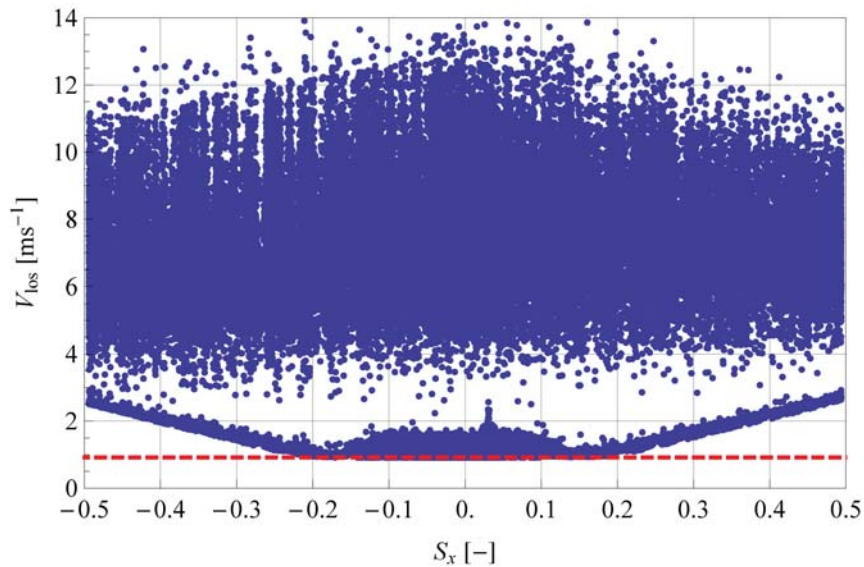


Figure 21: The line-of-sight speed vs the lateral scan pattern location  $S_x$ .

In the following figure the simulated radial speeds that correspond to blade signals are presented for the whole area of the scanning pattern (see also Figure 14). On the left, the radial speeds are presented with their sign, where it can be seen that negative speeds are appearing for the positive  $S_x$ , as expected due to the direction of rotation of the wind turbine's blade. On the right the absolute values of the radial speeds are presented, where it can be seen the symmetry around the y-axis of the distribution of the speeds.

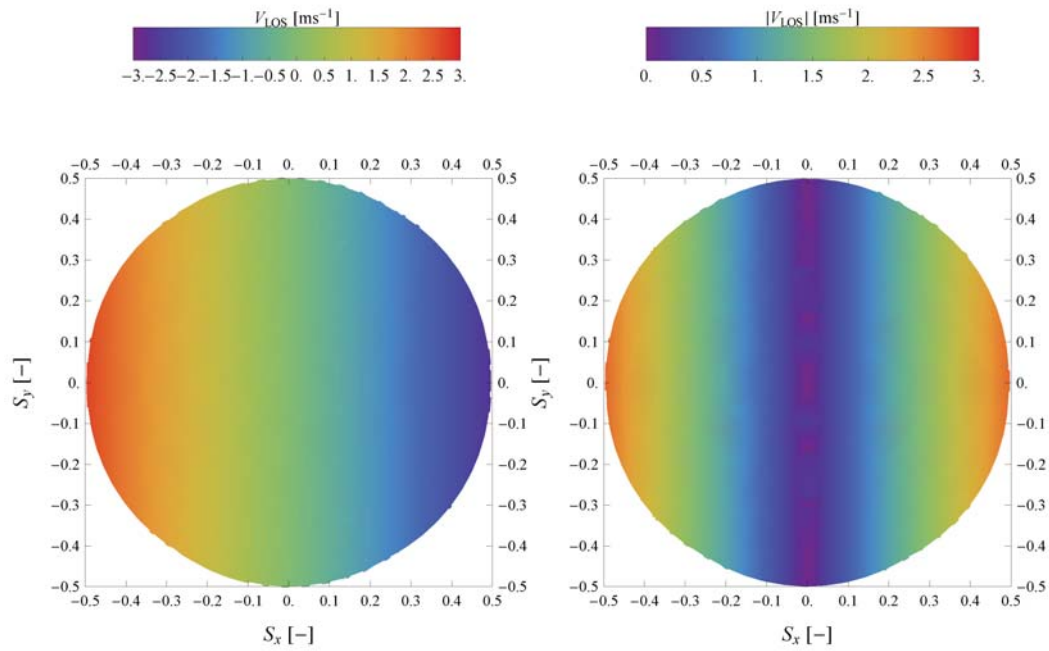


Figure 22: Simulated radial blade speeds as measured from a SpinnerLidar installed on the nacelle of a wind turbine, which is displaced vertically along the z-axis (see Figure 19) from the center of rotation of the wind turbine's blades.

#### 4.4.2. Model version 2

The model could also be expanded to take into account a lateral displacement  $l$  of the SpinnerLidar relative to the center of rotation of the wind turbine, which would lead to the following changes:

The Eq. 5 should become:

$$\mathbf{r} = \{d \cdot \tan\phi \cdot \cos\theta + l, d \cdot \tan\phi \cdot \sin\theta + h, d\} \quad (9)$$

and the Eq. 7:

$$\sin\theta_b = \frac{d \cdot \tan\phi \cdot \sin\theta + h}{r} \quad \text{and} \quad \cos\theta_b = \frac{d \cdot \tan\phi \cdot \cos\theta + l}{r} \quad (10)$$

Therefore in a similar way the Eq. 8 is becoming:

$$V_{LOS} = -S_x \cdot \omega \cdot h + S_y \cdot \omega \cdot l \quad (11)$$

In the Figure 23 the simulated blade speeds for a positive lateral displacement of + 1 m are presented (left), in comparison with the results of the Figure 22.

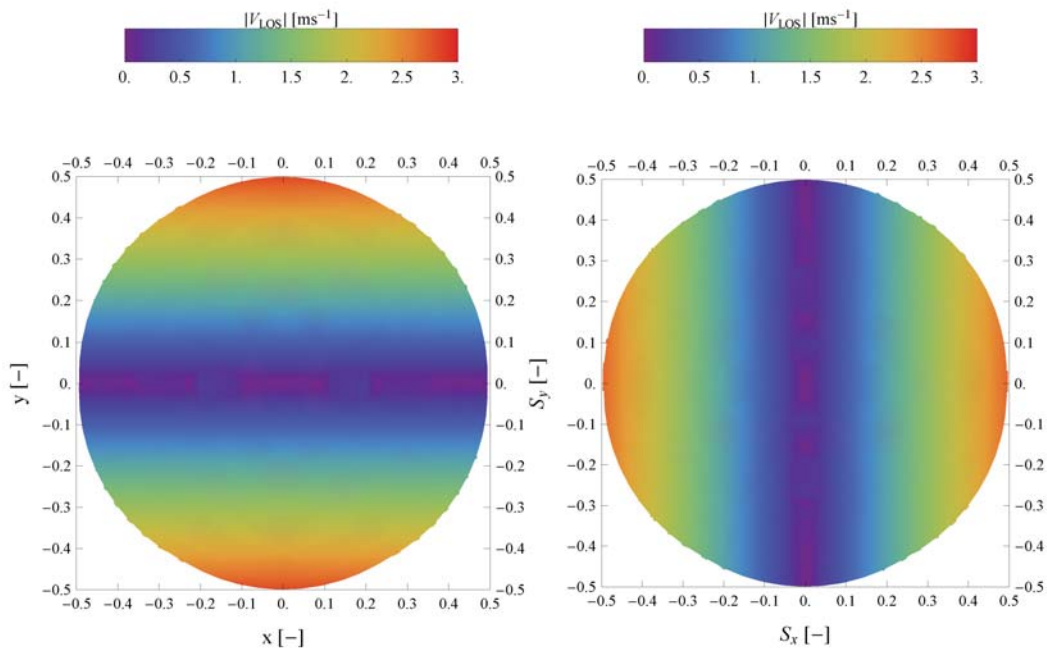


Figure 23: Simulated radial blade speeds as measured from a SpinnerLidar installed on the nacelle of a wind turbine, which is displaced horizontally along the y-axis (see Figure 19) from the center of rotation of the wind turbine's blades..

### 4.4.3. Alignment evaluation

In addition to the vertical and lateral displacement of the SpinnerLidar relative to the center of rotation of the wind turbine's blades, the speed amplitude of signals that originate from blades would be affected from potential offsets in the pitch ( $\alpha$ ), yaw ( $\beta$ ) and roll ( $\gamma$ ) angles of the SpinnerLidar. Such offsets would change the direction of the  $\mathbf{n}$  vector of line-of-sight of the SpinnerLidar and thus alter the expected blade return speed. These angles have been measured during the calibration and installation of the instrument on the wind turbine (see Table 6). However, the measured data offers a possibility for verifying those measurements. In order to evaluate them the following steps were followed:

- Apply 3 rotations around the axis  $x$ ,  $y$ ,  $z$  to the line-of-sight unit vector  $\mathbf{n}'$  (see Eq. 1)

$$\mathbf{n}'' = R_z(\gamma)R_y(\beta)R_x(\alpha)\mathbf{n}' \quad (12)$$

- Select all the 10 min periods where the mean wind speed was above  $8 \text{ ms}^{-1}$ . Based on geometry of the scanning pattern, above those speeds the radial wind speeds are larger than  $3 \text{ ms}^{-1}$  and therefore it is easy to distinguish them from the blade returns. In total 604 10-min periods were found and 600 were selected.
- Exclude those blade signals that originate for very low  $S_x$  and  $S_y$  values. This was required because as  $S_x$  approaches 0 the radial speed of the blade is also approaching 0. However as it have been mentioned in section 4.4.1 and presented in Figure 21, the SpinnerLidar cannot measure wind speed lower than  $0.92 \text{ ms}^{-1}$  and therefore those measurements are expected to be biased. Moreover when  $S_x$  and  $S_y$  are converging to 0 then the line-of-sight of the SpinnerLidar tends to get aligned with the pointing direction which results in additional noise in the data due to back reflections from a glass window that it is mounted on top of the scanner head of the SpinnerLidar.
- Construct a 5-parameter ( $h, l, \alpha, \beta, \gamma$ ) non linear model using the Eq. 8 and Eq. 11 and find the best fit parameters.

The time series of the best fit parameters are presented on the plots of the left column of Figure 24 and their mean values are presented in the following table.

	Measurement	Model 1	Model 2
$h$ [m]	1.75	1.89	1.89
$l$ [m]	-	0.03	0.00
$\alpha$ [°]	-0.89	0.07	-1.18
$\beta$ [°]	1.69	1.00	0.88
$\gamma$ [°]	0.30	6.28	0.00

Table 7: Measured and estimated offset angles and distance displacements of the SpinnerLidar relative to the axis of rotation of the wind turbine blades.

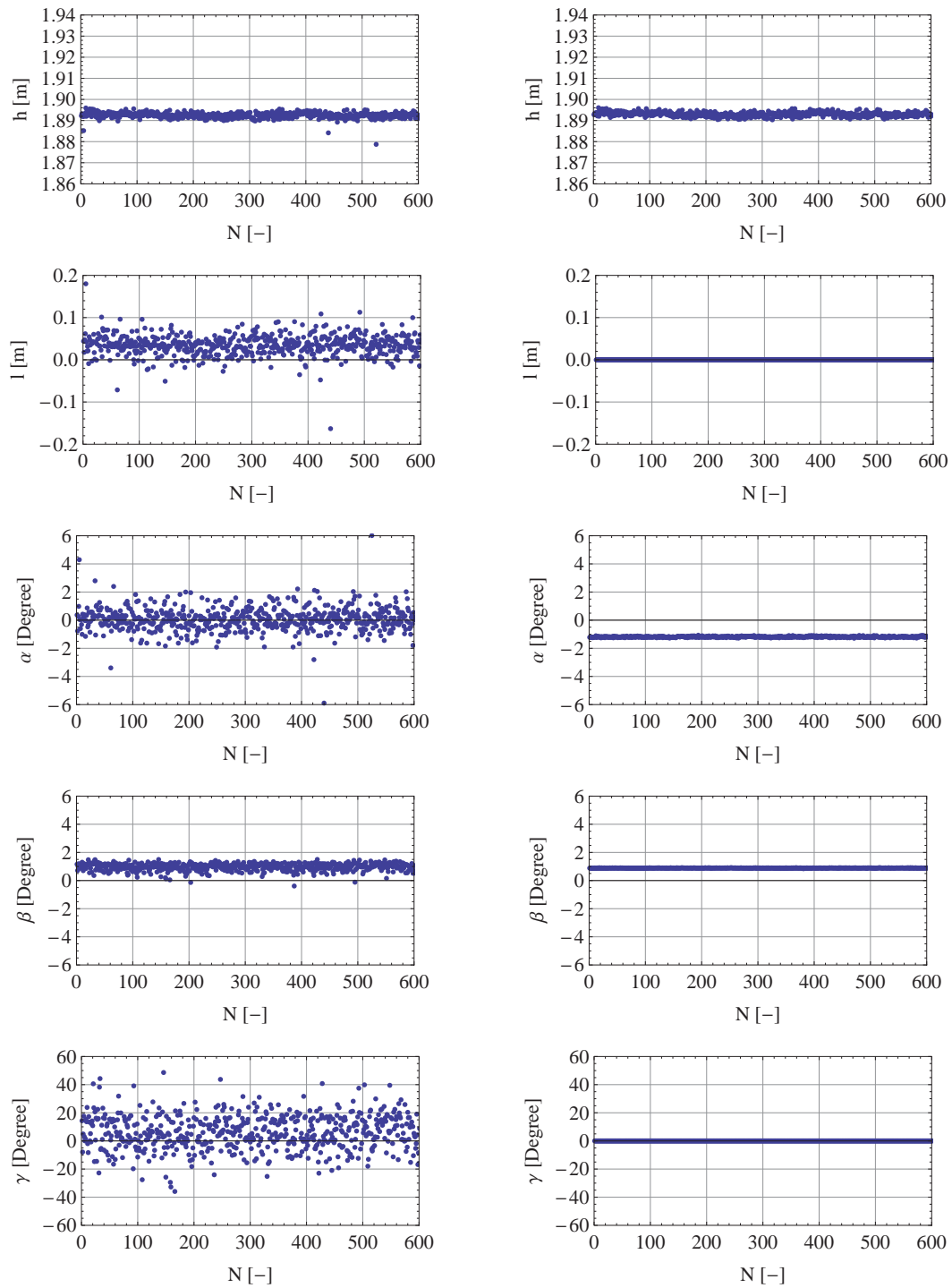


Figure 24: Results of the estimated offset angles and distance displacements of the SpinnerLidar relative to the axis of rotation of the wind turbine blades for 600 different 10-min periods. The left column presents the results when a non zero  $l$  is assumed and the right ones the opposite.

#### 4.4.4. Blade filtering algorithm

In order to construct a robust blade filtering algorithm the estimated offsets (both in direction and position) of the SpinnerLidar relative to the short-range WindScanner from the second implementation of the geometrical model (see Figure 24 (right column) and Table 7 (column *model 2*)), were used. For each of the 600 separately 10-min periods the expected blade radial speeds were simulated, using the rotational speed of the wind turbine rotor and compared to the measured ones. In Figure 25, the median absolute error, along with the estimated outer upper limit of the distribution of each 10-min period is presented (left plot) highlighted with blue and purple, respectively, and the corresponding histogram on the right.

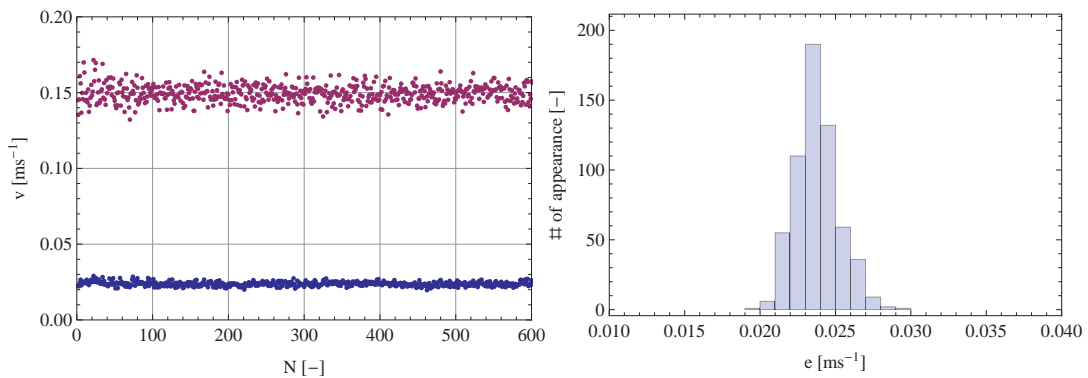


Figure 25: Estimated median value of the absolute error of the simulated radial blade speed in comparison to the measured ones (left) and the corresponding histogram (right).

Using the statistical results presented in Figure 25 a simple filtering algorithm was implemented, used to discriminate the wind speed signals from the blade radial signals.

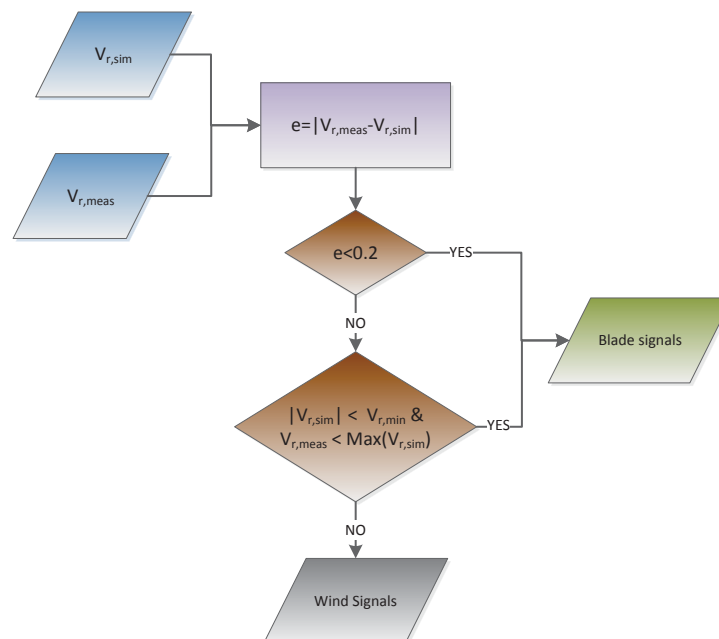


Figure 26: Architecture of blade filtering algorithm.

The architecture, presented in Figure 26, is based on 2 conditions: *a.* that the absolute difference of the estimated blade radial speed for a specific line-of-sight direction from the radial wind speed measurement is lower than  $0.2 \text{ ms}^{-1}$  and *b.* that the absolute of the estimated blade radial speed for a specific line-of-sight direction from the radial wind speed measurement is lower than the minimum detectable radial speed of the SpinnerLidar and the radial wind speed measurement is lower than the maximum simulated blade signal. If these two conditions are fulfilled then the measurement of the SpinnerLidar is indexed as a blade signal.

An example of the implementation of such a blade filtering algorithm is presented in Figure 27. In the top plot the values of the  $S_x$  and  $S_y$  components of the line-of-sight of the SpinnerLidar, during a full scan are presented. The corresponding radial wind speed measurements are presented in the plot below, along with the simulated blade signals. When implementing only the first condition (*a.*) of the blade filtering algorithm then it appears that a part of the blade radial speeds are detected (highlighted with red in the second from the bottom plot). The ones failed to recognized are the ones corresponding to speeds lower than the minimum measurable wind speed from the SpinnerLidar. In the bottom plot with red are highlighted the indexed blade radial speeds after taking into account both conditions in the filtering algorithm.

The resulted data availability after the implementation of the blade filtering algorithm is presented in Figure 35.

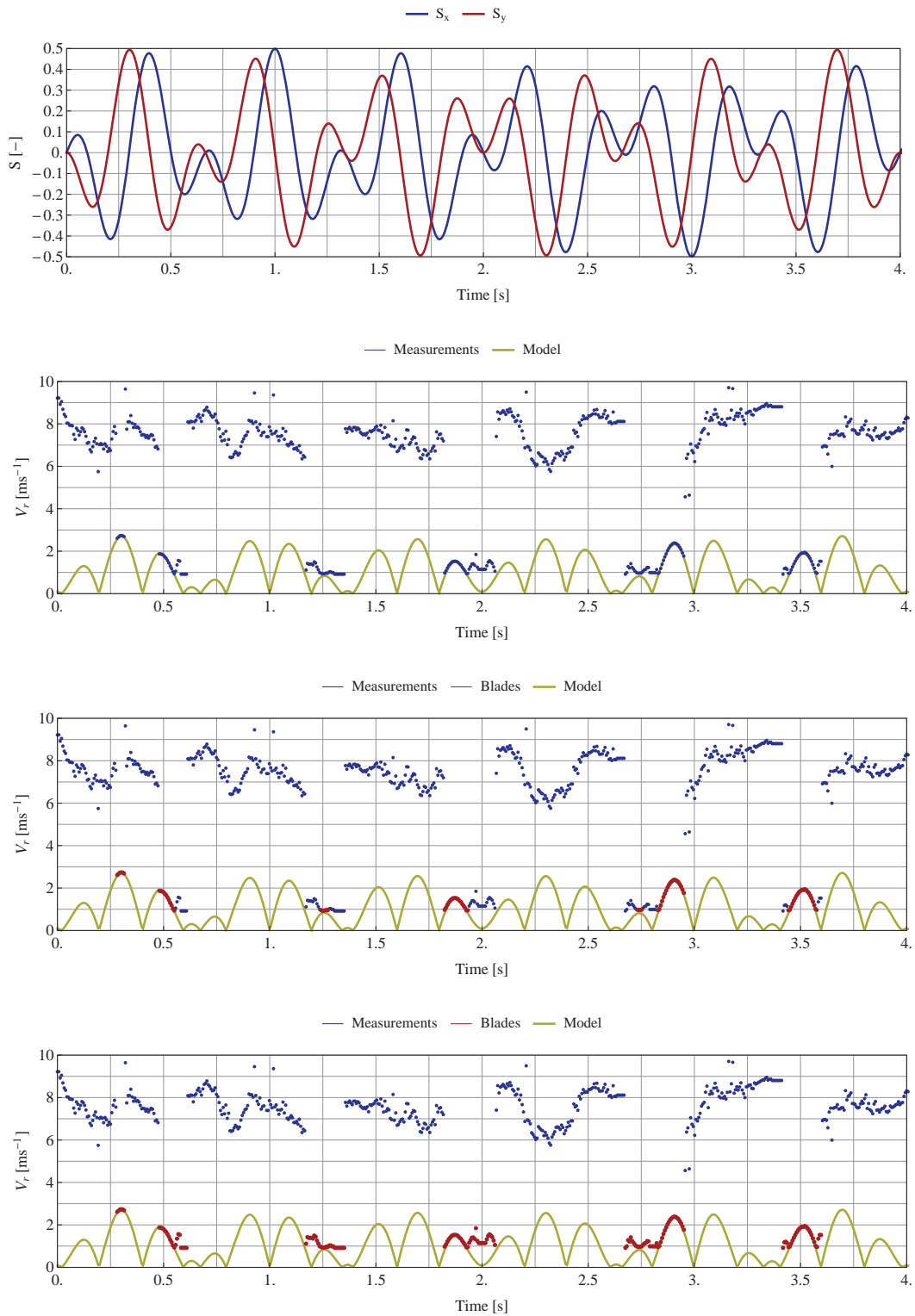


Figure 27: Example of the implementation of the blade filtering algorithm.



### 4.5.2. Sampling rate

The Doppler spectra were averaged together such that the sampling rate of wind speeds was for most of the campaign 156.25 Hz except from measurements at the end of the campaign after 2014-09-16, when trials with higher rates were run, i.e. 312.5 Hz as can be seen in Figure 30. The sampling rates of the wind speed were selected such that the scan patterns with duration 4 s and 2 s, respectively contained an integer number of samples.

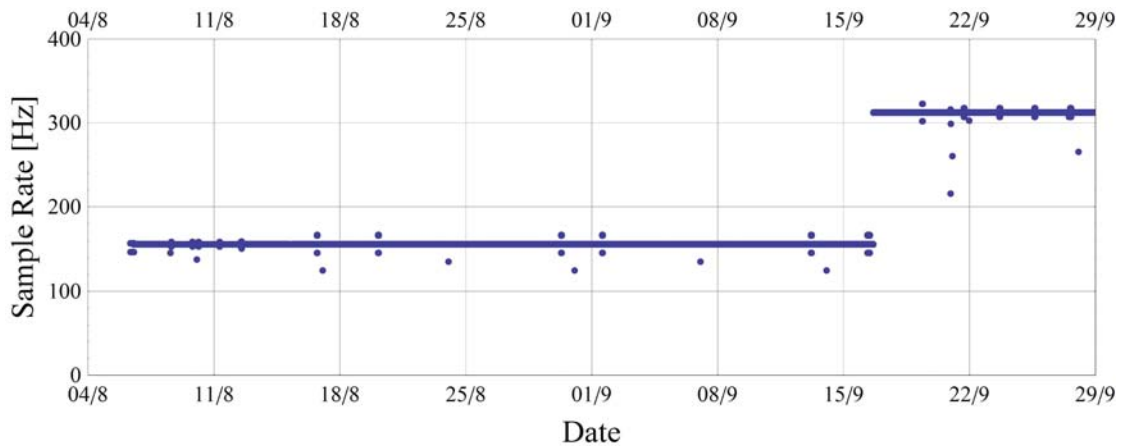


Figure 30: Overview of the sample rate.

### 4.5.3. Scan duration

The motor rotation speed was for most of the campaign 504 rpm which generates a complete scanning pattern in 4 s which with a sampling rate of 156.25 Hz gives 625 samples during 4 s. However, during the starting day 2014-08-06 between 08:33 and 13:03 the motor rotation speed was 500 rpm corresponding to a time of 4.032 s for the completion of the scanning pattern. Between 2014-09-16 and 2014-09-21 the rotation

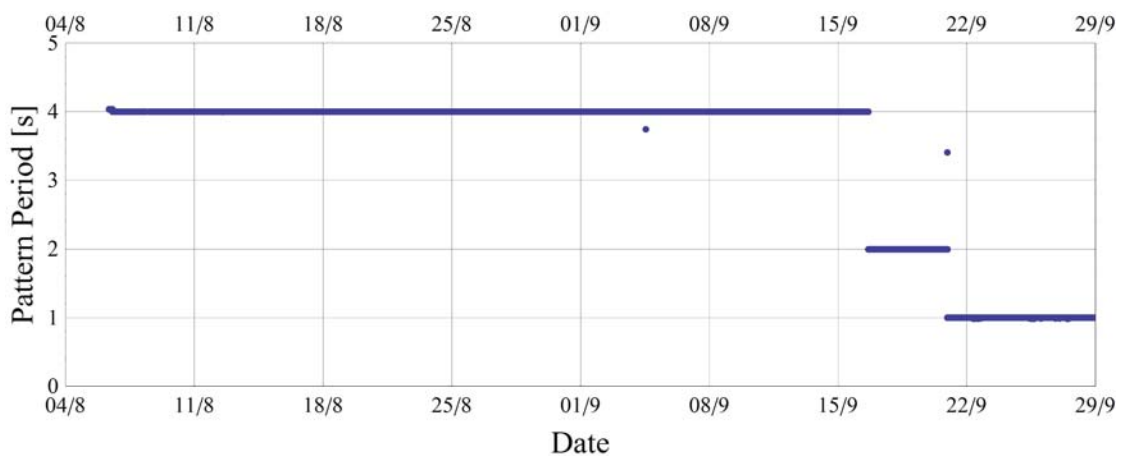


Figure 31: Overview of the time for completing the scanning pattern.

speed was at an elevated speed of 1008 rpm corresponding to a scan duration of 2 s as can be seen in Figure 31. From 2014-09-21 a trial with even higher rotation speed of 2016 rpm corresponding to a scan duration of only 1 s was tested, but the software implementation present at the time of the measurements did not cope with the demands.

#### 4.5.4. Line-of-sight speed, Signal strength and Quality

Here is an overview of the one-minute averaged line-of-sight speeds, Figure 32, signal strength, Figure 33, and quality measure, Figure 34, is provided. Please, note that it is the average of all samples without any removal of blade returns etc.

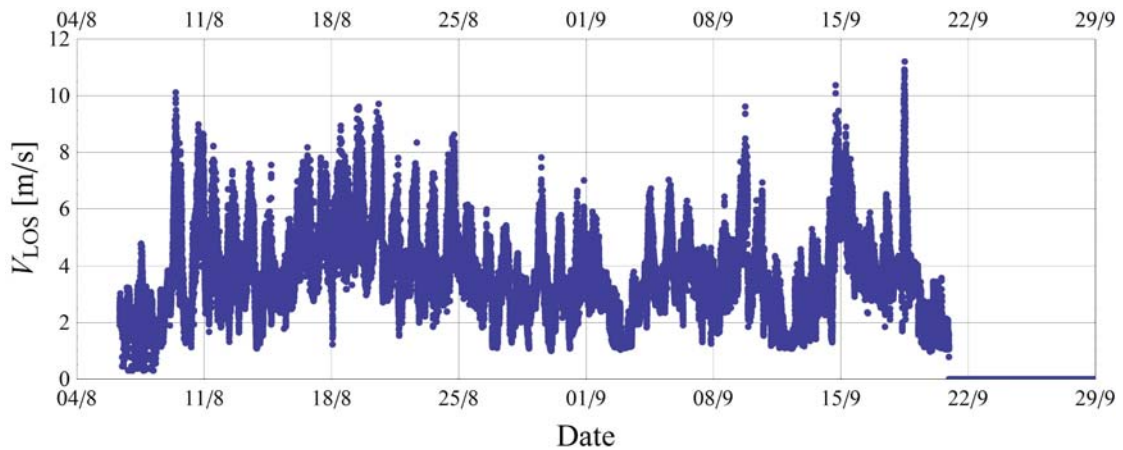


Figure 32: The one minute averages of the line-of-sight wind speeds of all samples.

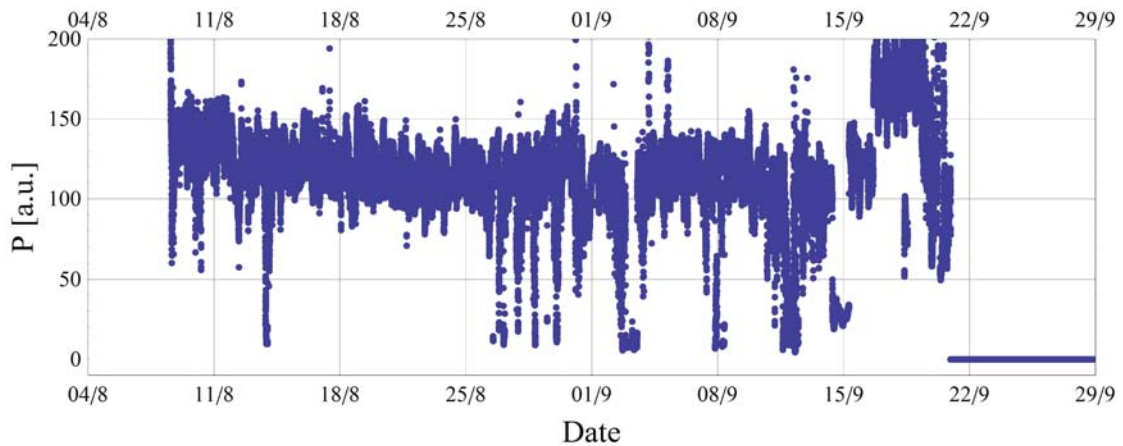


Figure 33: The one minute averages of the signal power of all samples.

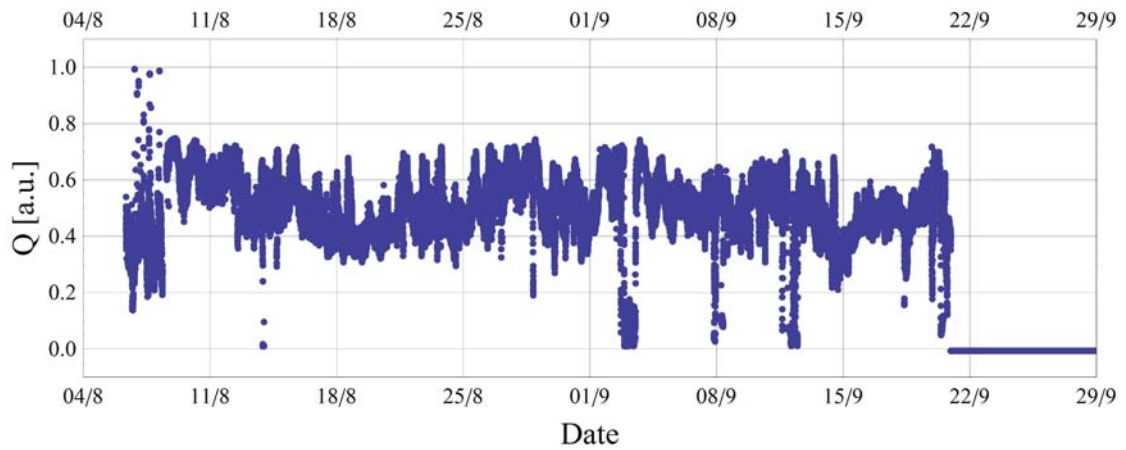


Figure 34: The one minute averages of the quality factor of all samples.

#### 4.5.5. Data availability after blade filtering

In the following figure the time series of the data availability of the SpinnerLidar data, after filtering out the blade signals is presented.

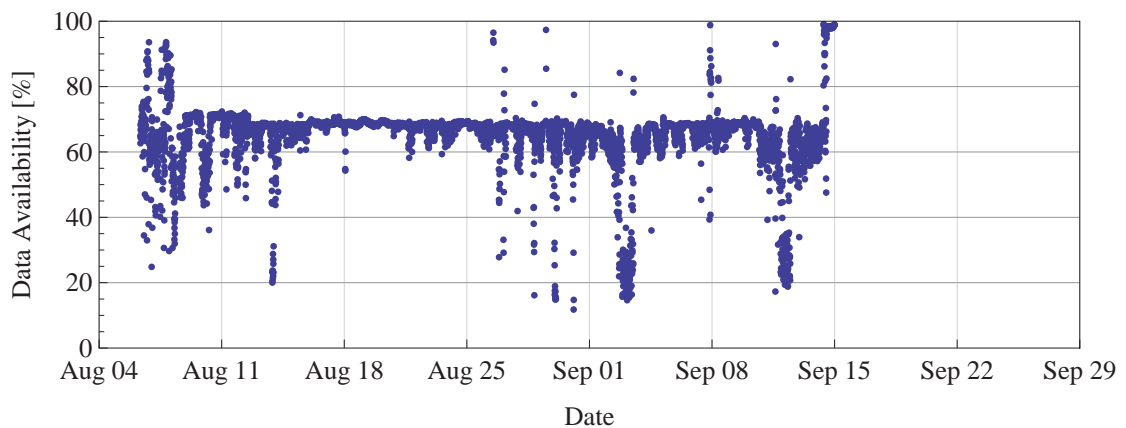


Figure 35: Data availability after filtering out speed measurements originated from the wind turbine's blades.

## Acknowledgments

The work presented herein is a part of the Danish Innovation Fund project titled *UniTTe - Unified testing procedures for wind turbines through inflow characterization using nacelle lidars*, Grant No. 1305-00024A.

## References

- [1] C. J. Karlsson, F. Å. A. Olsson, D. Letalick, and M. Harris. All-fiber multifunction continuous-wave coherent laser radar at 1.55  $\mu\text{m}$  for range, speed, vibration, and wind measurements. *Appl. Opt.*, 39(21):3716–3726, Jul 2000.
- [2] T. Mikkelsen, M. Courtney, I. Antoniou, and J. Mann. Wind scanner: A full-scale laser facility for wind and turbulence measurements around large wind turbines. In *Conference proceedings (online)*. European Wind Energy Association (EWEA), 2008.
- [3] M. Sjöholm, A. Pedersen, N. Angelou, F. Foroughi Abari, T. Mikkelsen, M. Harris, C. Slinger, and S. Kapp. Full two-dimensional rotor plane inflow measurements by a spinner-integrated wind lidar. In *Conference proceedings (online)*. European Wind Energy Association (EWEA), 2013.
- [4] C. M. Sonnenschein and F. A. Horrigan. Signal-to-noise relationships for coaxial systems that heterodyne backscatter from the atmosphere. *Appl. Opt.*, 10(7):1600–1604, Jul 1971.

## Appendix A Short-range WindScanner database

The data are stored in different database tables, based on the day of acquisition. The format of the tables is described by the following list:

1. **Date (YYYY-MM-DD HH:MM:SS)** Date and time based on the clock of the short-range WindScanner computer. Throughout the period of the measurement campaign the computer clock was being synchronized with the GPS network once a week. Thus time offsets between the short-range WindScanner measurements and measurements acquired from other instruments may be observed.
2. **Microsecond (Microseconds)**  
The microsecond timer value corresponding to the *Date*.
3. **X (m)**
4. **Y (m)**
5. **Z (m)**  
X,Y,Z coordinates of the location of a measurement ...
6. **Grid X (-)**
7. **Grid Y (-)**
8. **Grid Z (-)**  
... and corresponding grid cell indeces
9. **Vr2d1 (ms<sup>-1</sup>)**
10. **Vr2d2 (ms<sup>-1</sup>)**
11. **Vr2d3 (ms<sup>-1</sup>)** The radial wind speed measurements acquired from each one short-range WindScanner
12. **u (ms<sup>-1</sup>)**
13. **v (ms<sup>-1</sup>)**
14. **w (ms<sup>-1</sup>)**
15. **Vvector (ms<sup>-1</sup>)**
16. **Vdir (degree)**  
The amplitude and direction of the wind vector, along with the individual u,v,w components of the wind, where the u component is aligned with the direction from the wind turbine to the two met masts (283° from the North)
17. **Scan Index (-)**

- 18. Scan Turn (-)**
- 19. Scan Iter (-)** The scan index, turn and iteration values.
- 20. DataPointsInGridR2D1 (-)**
- 21. DataPointsInGridR2D2 (-)**
- 22. DataPointsInGridR2D3 (-)** Number of measurements acquired per grid cell
- 23. Vdir NS (degree)** The corrected direction of the wind vector (0° points to N)

## Appendix B Time lag in the short-range WindScanner data

Date	ScanIndex	TimeLag
201408060815	1	76.271186
201408211016	1	77.586207
201408251038	1	110.526316
201409250923	1	138.461538
201409271209	1	137.288136
201409271348	1	138.461538
201409271526	1	137.288136
201410021359	1	137.288136
201410291657	1	0.000000
201410291800	1	0.000000
201410291903	1	15.254237
201410292006	1	0.000000
201410292109	1	0.000000
201410292212	1	442.372881
201410292315	1	-900.000000
201410301021	1	0.000000
201410301123	1	15.254237
201410301226	1	15.254237
201410301329	1	0.000000
201410301433	1	0.000000
201410301536	1	0.000000

Table 8: Time lag in the scanning pattern  $l$  of the short-range WindScanner data relative to the met mast.

Date	ScanIndex	TimeLag
201408060847	2	91.525424
201408060953	2	91.525424
201408201358	2	91.525424
201408201504	2	91.525424
201408201611	2	91.525424
201408211154	2	91.525424
201408211300	2	91.525424
201408211407	2	91.525424
201408211514	2	91.525424
201408211620	2	91.525424
201408251216	2	91.525424
201408280030	2	91.525424
201408280137	2	91.525424
201408280244	2	61.016949
201408280350	2	91.525424
201408280457	2	91.525424
201408280603	2	91.525424
201409250955	2	152.542373
201409251101	2	152.542373
201409251208	2	152.542373
201409251315	2	152.542373
201409251421	2	152.542373
201409251528	2	152.542373
201409251635	2	152.542373
201409271420	2	152.542373
201410021431	2	152.542373
201410291729	2	0.000000
201410291832	2	0.000000
201410291935	2	30.508475
201410292038	2	0.000000
201410292141	2	91.525424
201410292244	2	-152.542373
201410301052	2	30.508475
201410301155	2	30.508475
201410301258	2	30.508475
201410301402	2	0.000000
201410301505	2	0.000000

Table 9: Time lag in the scanning pattern 2 of the short-range WindScanner data relative to the met mast.

Date	ScanIndex	TimeLag
201408060918	3	70.270270
201408061024	3	70.270270
201408201322	3	75.675676
201408201428	3	70.270270
201408201535	3	70.270270
201408201642	3	70.270270
201408211118	3	70.270270
201408211225	3	70.270270
201408211331	3	70.270270
201408211438	3	70.270270
201408211544	3	64.864865
201408251141	3	70.270270
201408280101	3	70.270270
201408280208	3	70.270270
201408280314	3	70.270270
201408280421	3	70.270270
201408280528	3	70.270270
201409251026	3	124.324324
201409251132	3	124.324324
201409251239	3	124.324324
201409251346	3	124.324324
201409251452	3	118.918919
201409251559	3	118.918919
201409251705	3	118.918919
201409271312	3	124.324324
201410021502	3	131.428571

Table 10: Time lag in the scanning pattern 3 of the short-range WindScanner data relative to the met mast.

## Appendix C SpinnerLidar database format

### C.1 The SpinnerLidar Data

The SpinnerLidar data of the first measurement campaign of UniTTe WP3 are available in the veadbs-03 database table *nordtank.spinnerlidarunitte*.

The three first columns deal with the time of the measurement. The first column is called "Name" which is the time including year, month, date, hour and minute, e.g., 201408060832. The second column is called *scan\_id*, and counts each measurement sample from 1 up to the number of measurements completed during all the complete scan patterns during the minute specified by the "Name". The third and last column dealing with the time is called "T" and is the time (s) from the start of the current scan pattern.

The measurement location is determined by the columns 5 (*Sx*), 6 (*Sy*), and 7 (*Sz*) together with the column 19 (Focus D). *Sx*, *Sy*, and *Sz* are the projections of the unit vector along the line-of-sight measurement direction on the SpinnerLidar internal x-axis, y-axis, and z-axis, respectively. FocusD is the distance (m) from the SpinnerLidar to the point where the measurement laser beam is focused.

The column 8 (*ws*) contains the wind speed ( $m s^{-1}$ ) component along the line-of-sight measurement direction.

The column 9 (*Q*) and column 10 (Power) might be of interest for screening purposes.

The rest columns are used for monitoring the operation of the instrument and they are not useful for the end-user of the data from this particular campaign.

#### C.1.1 The data columns

1. **Name (YYYYMMDDHHMM)**  
Date and time based on the clock of the SpinnerLidar computer.
2. **scan\_id**  
Counter incrementing for each sample. Resets every minute.
3. **Azim**  
Azimuth angle of the instrument. Important when the SpinnerLidar is rotating together with the turbine. During this campaign the SpinnerLidar was fixed on top of the nacelle.
4. **T**  
The time (s) from the start of the current scan pattern.
5. **Sx**  
The projection of the unit vector along the line-of-sight measurement direction on the SpinnerLidar internal x-axis.
6. **Sy**  
The projection of the unit vector along the line-of-sight measurement direction on the SpinnerLidar internal y-axis.

7. **Sz**  
The projection of the unit vector along the line-of-sight measurement direction on the SpinnerLidar internal z-axis.
8. **ws**  
The wind speed (m/s) component along the line-of-sight measurement direction.
9. **Q**  
A quality measure ( $0 \leq Q \leq 1$ ) of the speed estimate. It is defined as the ratio between the signal power around (+/- 1 bin) the estimated frequency of the thresholded Doppler spectrum +/- 1 bin, to the total signal power in the whole thresholded Doppler spectrum.
10. **Power**  
The total signal power in the whole thresholded Doppler spectrum.
11. **RT**  
Parameter for internal instrument diagnostics.
12. **RioRT**  
Parameter for internal instrument diagnostics.
13. **Acc0f**  
The voltage of the accelerometer channel 0.
14. **Acc1f**  
The voltage of the accelerometer channel 1.
15. **Acc2f**  
The voltage of the accelerometer channel 2.
16. **Acc3f**  
The voltage of the accelerometer channel 3.
17. **Acc0**  
The voltage of the accelerometer channel 0.
18. **Acc1**  
The voltage of the accelerometer channel 1.
19. **FocusD**  
The distance (m) from the SpinnerLidar to the point where the measurement laser beam is focused.
20. **TAI(LSB)**  
Parameter for internal instrument diagnostics.
21. **CPPR1**  
Counter (1count/10ns) which is reset once per revolution of the lower prism.

22. **DPPR1**  
The CPPR1 counter value at the last reset, i.e. the duration measured in counts of the last revolution of the lower prism.
23. **CPPR2**  
Counter (1count/10ns) which is reset once per revolution of the upper prism.
24. **DPPR2**  
The CPPR2 counter value at the last reset, i.e. the duration measured in counts of the last revolution of the upper prism.
25. **CPPP**  
Counter (1count/10ns) which is reset once per completed scan pattern, i.e. when both CPPR1 and CPPR2 are reset at the same time.
26. **DPPP**  
The CPPR counter value at the last reset, i.e. the duration measured in counts of the last complete scan pattern.
27. **Sx\_2**  
Not used in this experiment.
28. **Sy\_2**  
Not used in this experiment.
29. **Sz\_2**  
Not used in this experiment.
30. **time**  
Parameter for internal instrument diagnostics.
31. **CPPS**  
The counter (1count/10ns) internally used for the synchronization between data stream of prism positions and the data stream of line-of-sight wind speeds. The reset of the CPPS is based on prism counter in order to fulfill the laser safety requirements. If the period between resets is too long, the instrument stops the emission of laser radiation.
32. **Qlength**  
Parameter for internal instrument diagnostics.

**DTU Wind Energy**  
**Department of Wind Energy**  
Technical University of Denmark

Frederiksborgvej 399  
DK-4000  
Roskilde

<http://www.vindenergi.dtu.dk>